The Canadian Mineralogist
Vol. 33, pp. 243-259 (1995)

APPLICATIONS OF AUGER-ELECTRON SPECTROSCOPY TO GEOCHEMISTRY

H. WAYNE NESBITT AND ALLEN R. PRATT

Department of Earth Sciences, University of Western Ontario, London, Ontario N6A 5B7

ABSTRACT

The composition of the uppermost 50 Å of mineral surfaces is readily determined by Auger electron spectroscopy (AES). Lateral resolution (analytical spot-size) less than 1 μm can be achieved routinely, and the concentration of most elements can be quantitatively determined at levels as low as one-quarter to one weight percent. Auger instruments typically include an ion sputter-gun, which provides the means to obtain Ångström-scale quantitative compositional depth-profiles of the near-surface zones of minerals. Compositional depth-profiles through air-oxidized pyrrhotite surfaces are reported here, and demonstrate that Fe diffuses rapidly from the bulk to the surface of pyrrhotite grains during oxidation by air. Auger results of a goethite surface, combined with electron-microprobe results, demonstrate that Al is distributed throughout the bulk of the mineral, and that Ni is concentrated at the surface (uppermost 50 Å). Sensitivity factors for Fe and O in goethite are derived from the data. The surface sensitivity of AES, its high spatial resolution, and the ability to obtain compositional depth-profiles, yield an exceedingly powerful tool to study the near-surface regions of minerals. The technique is a boon to experimental petrologists and geochemists in that detection of Ångström-thick leached veneers and authigenic overgrowths helps circumvent the ever-present problem of slow rates of reaction.

Keywords: Auger spectroscopy, surface analysis, depth profiling, mineral surfaces, surface compositions, reaction rates, reaction mechanisms.

SOMMAIRE

On peut facilement obtenir la composition de la couche à 50 Å de la surface des minéraux par spectroscopie des électrons Auger. Avec cette technique, on obtient une résolution latérale (diamètre du faisceau) de moins de 1–2 μm, atteinte de façon routinière, et la concentration de la plupart des éléments, quantifiée à un niveau du quart d'un pourcent à un pourcent. Les instruments Auger possèdent, en général, un canon pour ablation ionique, ce qui permet d'obtenir, à l'échelle de l'Ångström, un profil compositionnel en profondeur dans la couche superficielle des minéraux. De tels profils d'un échantillon de pyrrhotite oxydé dans l'air montrent que le Fe diffuse rapidement de l'intérieur vers la surface au cours de l'oxydation. Des études semblables de la surface de la goethite, préalablement examinée par microsonde électronique, démontrent que l'aluminium est distribué uniformément dans l'échantillon, et que le nickel, par contre, est concentré dans la couche externe de 50 Å. On peut dériver des facteurs de sensibilité pour les atomes Fe et O dans la goethite à partie de ces données. La sensibilité de la spectroscopie des électrons Auger à la constitution de la surface, ainsi que la possibilité d'obtenir un profil de la composition en fonction de la profondeur, en font un outil vraiment puissant pour caractériser les régions de surface des minéraux. La technique est particulièrement utile à ceux qui s'attardent à l'étude de minéraux par pétrologie et géochimie expérimentales; la caractérisation de couches lessivées de quelques Ångströms d'épaisseur en surface et de surcroissances authigènes fournit une solution au problème omniprésent de taux de réaction très lents.

(Traduit par la Rédaction)

Mots-clés: spectroscopie des électrons Auger, analyse de la surface, profils en profondeur, surface de minéraux, composition de la surface, taux de réaction, mécanismes de réaction.

INTRODUCTION

Observation of Auger electrons was first reported by Auger (1925) through the study of particle tracks in cloud chambers. Auger spectroscopy has received less attention than other types of spectroscopy until recently, primarily because the Auger process and Auger electrons were viewed more as an impediment to the quantification of other processes (*e.g.*, fluorescence yields and modeling of X-ray lines) than as a technique to obtain compositional and chemical-state information about gases and solids. As a result, understanding of the Auger process grew more as a result of its "nuisance value" than of any desire to develop it as an analytical method.

Corrosion, metallurgical and semiconductor studies have increased sharply during the last 30 years, and with these studies there has been an increased need for

accurate compositional analysis of surfaces and interfaces. Auger electrons are derived from within the near-surface region of solids (the uppermost 50 Å), and reflect the elemental concentrations of the surface region; consequently, Auger applications and instrumentation have developed rapidly in the last three decades (*e.g.*, Lander 1953, Scheibner & Tharp 1967, Weber & Peria 1967, Palmberg *et al.* 1969, Wells & Bremer 1969). Auger spectroscopy now is recognized as fundamentally important to the comparatively new field of Surface Science because of its surface sensitivity. Application of Auger spectroscopy now includes study of ionization of gases, chemical-state properties of molecular ions, catalysis and interactions occurring at solution–mineral interfaces. This last aspect is particularly important to geochemistry, and is emphasized here.

We present a brief review of the fundamental aspects of the Auger process and comment on the advantages and disadvantages of Auger spectroscopy relative to other techniques. Applications presented here emphasize measurement of surface compositions of oxides and sulfides, and compositional depth-profiles of these phases. There are numerous reviews of the theory related to generation of Auger ions (Burhop 1952, Mehlhorn 1970, Sevier 1972, Burhop & Assad 1972, Carlson 1975, Briggs & Seah 1990), reviews of instrumentation (Briggs & Seah 1990), and reviews of geochemical applications (Hochella 1988, Hochella *et al.* 1988, Mogk 1990). There is no attempt to incorporate the aspects covered by these excellent reviews. Instead, reference is made to them throughout the text, and they should be consulted for additional, detailed information on Auger spectroscopy. The emphasis here is on collection, quantification and interpretation of compositional depth-profiles of geological materials.

Theory of Auger and Related Processes

Introduction

A recent detailed review of the theory is given in Briggs & Seah (1990). Energy levels of electrons in an atom can be divided into valence (outer) and core (inner) levels (or shells), as in Figure 1. Valence electrons are affected both by the nucleus of the atom with which they are associated (henceforth referred to as the central atom), and by neighboring atoms or ions surrounding the *central* atom. Core electrons are "closer" to the nucleus of the central atom than are valence electrons, and hence are strongly affected by the charge on the nucleus; however, they are also affected by ions and atoms of the surrounding environment. Bombardment of solids by X rays or electrons may dislodge core electrons from their inner shells ($L_{2,3}$, L_1 or K shells of Fig. 1), and they may either escape the surface of the solid (if the central atom is sufficiently close to the surface) or they may be incorporated into neighboring ions. Readjustment of the central ion occurs rapidly after dislodgment of the core electron, and one of these adjustments includes the Auger process.

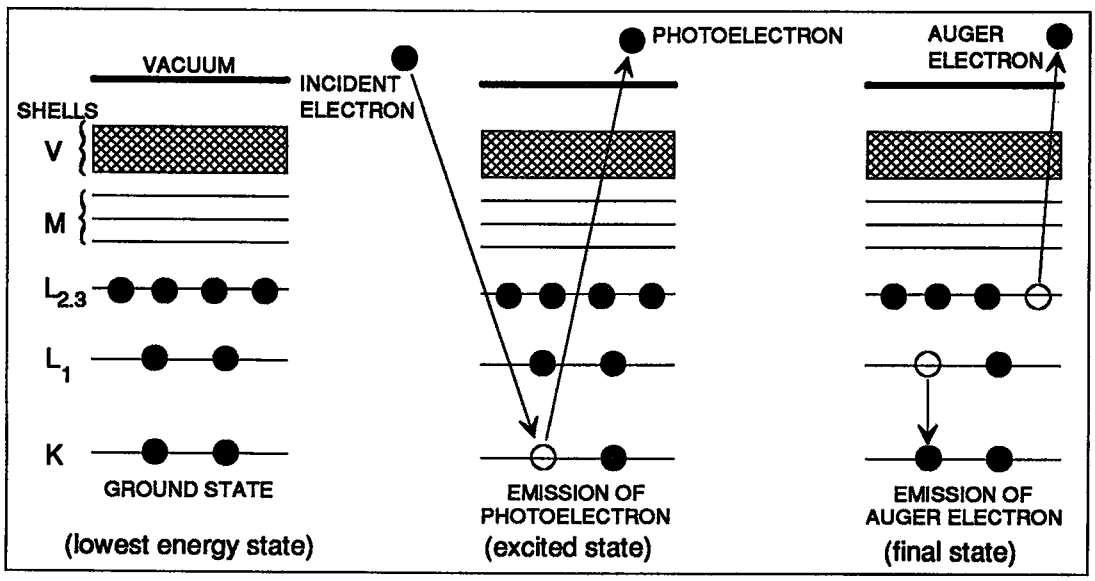

FIG. 1. Generation of Auger electrons and photoelectrons. The hatched areas represent numerous valence shells containing valence electrons, and the large dots represent core electrons filling inner shells. The circles represent holes (vacated by electrons). The labels V, M, $L_{2,3}$, $L1$ and K represent electron orbitals.

Photoelectron spectroscopy

The energy required to dislodge a core electron may be derived from X rays (photon) or from electrons with high kinetic energy (Fig. 1, incident electron). The energy imparted to a core electron (Fig. 1, *K*-shell core electron) must be greater than the energy binding the electron to the nucleus, otherwise the electron remains in its shell rather than being ejected. In fact, the energy of the incident electron must be approximately five times greater than the binding energy to obtain removal of appreciable quantities of core-level electrons. The ejected electron is called a photoelectron (Fig. 1). Their study is the domain of *Photoelectron Spectroscopy*; where the energy source is a beam of X rays (photons), the field of study is X-ray Photoelectron Spectroscopy (XPS).

Auger spectroscopy

After emission of a core electron, the resulting ion is energetically unstable (Fig. 1, excited state), and the remaining electrons are rapidly rearranged. The ion may achieve a lower energy-state, although not ground state, by having another core electron jump from a higher-level inner shell (Fig. 1, L_1 shell) to the vacated site in the lower-level shell (Fig. 1, *K* shell). The jump is energetically favored because electrons in higher-level shells have greater energy (potential and kinetic) than electrons in lower-level shells. For our example, electrons of the L_1 shell have greater energy than electrons of the *K* shell. Upon transfer of an electron from the *L* to *K* shell, the excess energy resulting from the transfer is dissipated through one of two processes, emission of X rays or ejection of a second electron. Through ejection of a second electron, energy is dissipated dominantly in the form of kinetic energy of the ejected electron (Fig. 1, final state). This ejected electron is the Auger electron. After emission of the Auger electron, the atom lacks two electrons, one from each of the L_1 and $L_{2,3}$ shells, and hence has become a doubly-charged ion.

The transition from a neutral atom to one lacking two electrons is, for the example shown in Figure 1, referred to formally as a $KL_1L_{2,3}$ transition. Such a formalism requires the shell from which the photoelectron is emitted to be listed first. The shell from which the electron "jumps" to fill the vacancy created by the photoelectron is listed second, followed by the shell from which the Auger electron is ejected. If an Auger electron were emitted from a valence shell, the transition would be written KL_1V, or *KVV* if both the "jump" electron and Auger electron are derived from valence shells. The ejected Auger electron is derived either from the same shell as the "jump" electron or from a higher-energy shell (a shell farther removed from the nucleus).

The vacancy created by the "jump" or the Auger electron (or both) may also be filled by electrons from still higher energy-shells. The process may continue with newly created vacancies filled by additional "jump" electrons, and with energy dissipated by ejection of additional Auger electrons. With each electron lost, the net charge on the resulting ion increases; charges as high as +22 have been recorded (Pleasonton & Snell 1957).

A minimum of three electrons are associated with the production of an Auger electron (Fig. 1). From this, it is apparent that the Auger process does not occur in H and He. Auger electrons are generated from all other elements; consequently, Auger Spectroscopy can be used to detect almost all elements in the near-surface region of solids. This is a major advantage of the technique.

Properties of Auger electrons and X rays

The incident electron may penetrate a few micrometers into the solid and still dislodge core electrons. As a result, photoelectron, Auger and X-ray processes occur well beyond the near-surface of the solid. Whereas photons have sufficient energy to escape the solid from a depth of a few micrometers, photoelectrons and Auger electrons cannot penetrate more than a few atomic diameters from their site of generation. As a result, only photoelectrons and Auger electrons generated within the first few monolayers (approximately 50 Å) escape the solid to be detected by analyzers. This extreme attenuation of photoelectrons and Auger electrons results in exceptional sensitivity of Auger spectroscopy and X-ray photoelectron spectroscopy to surface layers.

Some incident electrons are reflected back toward the surface and laterally (back-scattered electrons), and generate additional Auger electrons after reflection. Those generated within a few monolayers of the surface escape and contribute to the Auger signal. As a result, the surface area from which Auger electrons are emitted is somewhat greater than the area on which the incident beam is focused.

The *escape depth* or *attenuation length* of Auger electrons is proportional to the mean-free-path of the Auger or photoelectron in the solid. Escape-depths of Auger electrons vary, depending upon the element from which the Auger electron was ejected and on the composition and crystallographic properties of the solid. There is much greater probability for the light elements to release energy through ejection of Auger electrons than through emission of X rays, but the probability decreases with increasing atomic number. There is approximately equal probability that arsenic will yield an Auger electron and a photon (X ray).

As mentioned previously, an ion in the excited state (Fig. 1, central diagram) may dissipate energy through

emission of X rays (photons) as well as Auger electrons. The energy lost by emission of a photon yields the final state for the ion without an increase of charge on the ion. Study of these X rays is the domain of X-ray fluorescence (XRF) spectroscopy. Once generated, X rays escape from a depth of many micrometers; in contrast to photoelectrons and Auger electrons, X rays are derived from a large volume of the solid, increasing the likelihood that the compositions obtained by XRF are representative of the entire sample. X-ray fluorescence spectroscopy is an important tool for determination of bulk compositions of solids.

Auger electrons from individual elements

Although many factors contribute to the energy of ejected Auger electrons (Briggs & Seah 1990, Chapters 1 to 3), the major contribution comes from the difference between the binding energy of an electron in the *K* shell (E_K) and the binding energies of electrons in the other shells involved in the transition (where binding energy is the energy binding the electron to the nucleus). The energy of the Auger electron in the example (Fig. 1) is approximately

$$E_{KL_1L_{2,3}} = E_K - E_{L_1} - E_{L_{2,3}} \quad (1)$$

where E_{L_1} and $E_{L_{2,3}}$ are the binding energies of electrons in the L_1 and $L_{2,3}$ shells (the signs of Eq. 1 assume that bound states have negative energy). Note that the energy $E_{L_{2,3}}$ is the energy after removal of the core electron from the atom. Although a simplification, the equation is useful for many applications of Auger spectroscopy. The correct expression for Auger energy includes three additional terms, that tend to cancel (Kim et al. 1976).

The kinetic energy of an emitted Auger electron is primarily a function of the energy levels of the atom involved in the Auger process (Eq. 1). As no two elements have identical orbital energies of the electrons, the binding energies of their electrons are likewise unique, and measurement of the kinetic energy of the Auger electron leads immediately to identification of the elements. In practice, identification is a matter of comparing an experimental result against spectra in atlases or tables of known spectra. Furthermore, there is a direct (but complex) relationship between the intensity of the Auger signal (number of counts) for a given transition and the abundance of the element in which the transition occurs; consequently, Auger spectroscopy can be used to obtain the composition of solid surfaces. Compositional analyses commonly are accurate to within 2% (relative to amount present) for optimal surfaces and 5–15% for rough, porous or otherwise unusual surfaces.

Instrumentation and Methodology

Instrumental design

The major components of the instrument are a primary beam (X-ray or electron source), an analyzer of electron energy to detect Auger electrons and measure their energies, an ion gun to sputter the surface of the sample, and an ultra-high vacuum system.

X-ray or electron beams can be used to generate Auger electrons, but the latter beam is preferable for two reasons. An electron beam can be much more intense than an X-ray beam, and the resulting Auger signal generally is correspondingly more intense. Most importantly, high-intensity primary electron beams can be focused to a submicrometric spot-size and still yield a sufficiently strong Auger signal to determine compositions of the surface. The electron beam can be used to analyze natural samples where grain size is highly variable. Advantages of X-ray primary beams include low background (compared with an electron beam) and minimal radiation-induced damage.

Cylindrical mirror analyzers (Palmberg *et al.* 1969, Wells & Bremer 1969, MacDonald 1970) have high collection-efficiencies and reasonable energy-resolution, and are the most common analyzers used today. High-resolution electron analyzers became available in the late 1960s and were the impetus for development of the current instruments [see Hochella (1988) for additional information].

X-ray and primary electron beams do not remove significant amounts of material from the surface of the solid; hence the technique is nondestructive. Inclusion of an ion gun with the instrument offers the user a very powerful tool to study changes to the composition of solids as a function of depth (on the Ångström scale). The technique is particularly useful where thin veneers of secondary products form on surfaces. Alternate sputtering and Auger analysis of the sputtered surface yields compositional depth-profiles, where the depth resolution is controlled by the rate of sputtering. The area sputtered is much larger than the analyzed area to avoid complications arising from the edges of the crater produced by sputtering.

As mentioned previously, the escape-depth of Auger electrons is small; consequently, a high vacuum (less than 10^{-9} torr) is required to ensure minimum attenuation of the Auger signal and little contamination of the sample surface during analyses. Hochella (1988) provided additional information about Auger vacuum systems.

Oxygen, carbon and nitrogen can be detected by Auger electron spectroscopy (AES) on the surfaces of most solids exposed to the atmosphere. Contamination dilutes the Auger signal of elements in the underlying solid, and is to be avoided if quantitative analyses of surfaces are required. Samples reacted in solutions may acquire a surface film of solutes as samples are

removed from solution and the solvent evaporates. For such circumstances, AES analyses may yield entirely erroneous results as to the nature and concentration of elements in the near-surface. With careful washing, the problem generally can be avoided.

The ultrahigh vacuum required to prevent attenuation of Auger electrons requires all samples to be properly dried and degassed before analysis. Therefore, the vacuum must be constantly monitored after insertion of new samples into the instrument. Some materials are unstable in vacuum and may require long periods of pumping to obtain a vacuum appropriate for analysis. As well, introduction of unstable solids into the instrument may cause degradation of the analytical system through formation of coatings on detectors and other parts. A recent review of instrumentation is given by Rivière (1990).

Sample preparation

Sample holders are made of a conducting material, commonly aluminum, to prevent charging of samples, and good electrical contact must be made between sample and holder. With good contact, charging during analysis is no problem for metals and semiconductors.

Insulators, such as silicate minerals, become charged during Auger analysis, rendering the results of the analysis useless. In electron-microprobe analysis, the bulk of the X rays are derived from a depth of a few micrometers; hence thin, conductive coatings are applied to surfaces to prevent charging without deleterious effects to analyses. Coatings generally cannot be applied to samples analyzed by Auger spectroscopy because Auger electrons are derived from the uppermost 50 Å; even exceptionally thin coatings (less than 10 Å) cause extreme dilution and attenuation of the Auger signal derived from the sample beneath a coating. There are, however, two important aspects affecting charging, the incident angle of the primary electron beam relative to the surface to be analyzed, and the operating conditions of the instrument. These can be modified to overcome charging of insulators in most studies. Mogk (1990) reviewed application of AES to weathered surfaces of silicate minerals; he recommended incident angles of 60° and 30°, a primary beam current of 20–50 nA and an accelerating voltage of 3 kV to prevent charging.

Auger Analyses of Solids

Surface textures and morphology

An Auger instrument with the capability to raster and focus the primary electron beam is referred to as a Scanning Auger Microscope (SAM); it has the capability to produce high-quality micrographs with resolution much greater than reflected- or transmitted-light microscopy, but less than scanning electron microscopy (SEM). The SEM-like capability, combined with the ability to carry out near-surface analyses and an analytical spot-size less than 1 μm in diameter, make Auger spectroscopy well suited to study geological materials where surfaces of grains are small.

Elemental analysis

Use of a focused primary electron beam to obtain high lateral resolution is achieved at the expense of comparatively low sensitivity (grossly comparable to sensitivity of the electron microprobe). Elements present at less than 0.1 to 0.5 atomic % generally cannot be detected by Auger spectroscopy; thus the technique is restricted to analysis of samples for major and minor elements of the near-surface. Although sensitivity may be increased in some situations using an X-ray primary beam, loss of resolution restricts X-ray source instruments to large surface-areas (mm to cm square solid surfaces).

Auger spectroscopy gives quantitative analyses for elements heavier than He. One to two atomic % of a monolayer of (or on) a solid generally can be measured, and for some elements, as little as 0.3 atomic % can be detected. Sensitivity generally decreases with increasing binding energy, and low-energy Auger peaks of individual elements are usually used for analytical purposes. The low-energy Auger processes also yield analytical results more indicative of the surface composition of solids (first few monolayers) because the escape-depth of low-energy Auger electrons is less than that of higher-energy Auger electrons.

The Auger signal for goethite (Fig. 2A) is typical of "integrated" Auger *survey scans* in that small Auger peaks are superimposed on a large background (of inelastically scattered electrons) that increases with increased kinetic energy. To circumvent the problems of quantifying these small peaks, *differentiated* survey-scans of the Auger signal are usually obtained (Fig. 2B) and used both for identification and quantitative analysis. By taking the derivative at each point of the Auger spectrum (counts as ordinate and kinetic energy as abscissa), the background is largely eliminated, and the Auger peaks are enhanced (Briggs & Seah 1990). Detailed discussion and quantification of the goethite survey-scan are provided in the applications section that follows.

Compositional depth-profiles

AES instruments, coupled with an ion gun, provide the capability to obtain compositional depth-profiles of solids at the Ångström scale, with lateral resolution of the order of a micrometer. Depth profiling is accomplished by alternately sputtering and analyzing the surface for elements of interest. The walls of the resultant crater may complicate the Auger analytical signal. To remove their effect, the ion beam is rastered over a

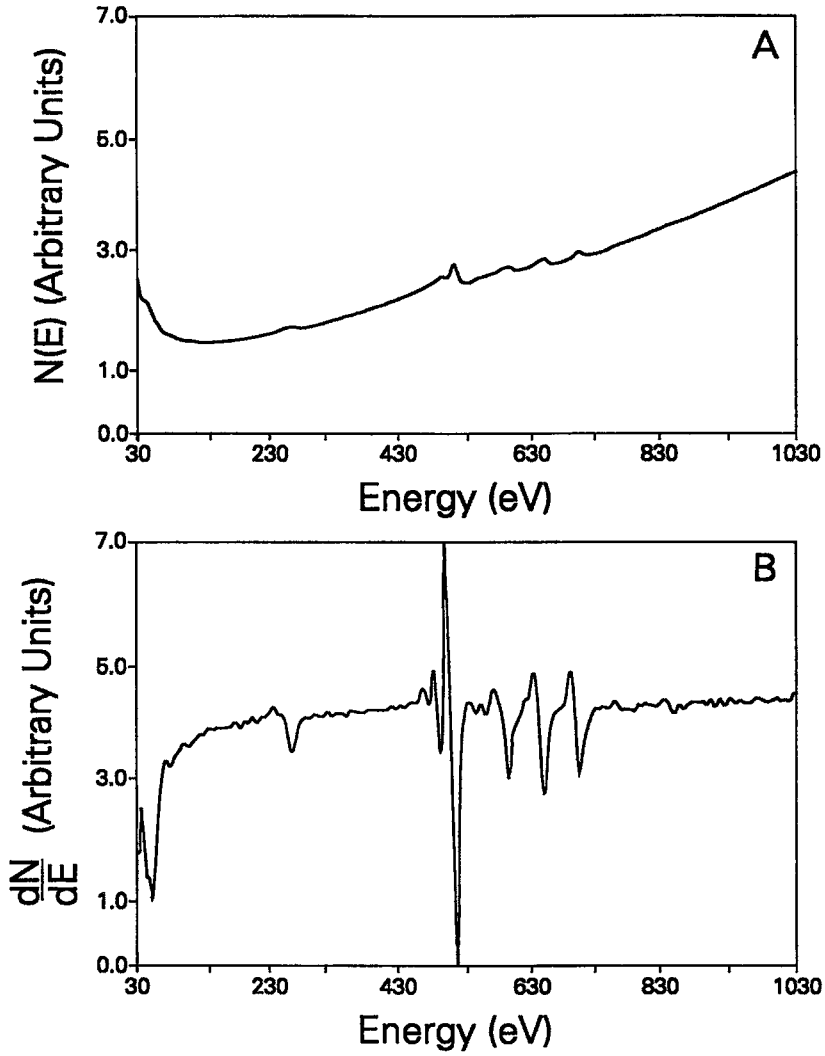

FIG. 2. An Auger spectrum of goethite over the kinetic energy range 30 to 1030 eV. (A) The integrated Auger spectrum; the analytical conditions are: 3.0 keV primary-beam accelerating potential, with a beam current of 25 nA and a primary beam-size of approximately 1 μm (lateral resolution). (B) The differentiated spectrum; this spectrum generally is used for identification of elements and to obtain atomic compositions of the near-surface of solids.

much larger region than the area to be analyzed. Although the analytical results obtained are not continuous with respect to depth, the ability to control depth of sputtering allows depth resolution as high as a few Ångströms. Depth of sputtering is controlled by varying the time of sputtering, or by altering the kinetic energy of the beam used for sputtering. Measurement of crater depth produced by sputtering provides the relation between sputtering time and depth, hence the information necessary to convert time of sputtering to depth of analysis (in Ångströms). Hofmann (1990) provided a thorough review of compositional depth-profiling using Auger instruments.

Sputtering of the surface by ion beams is not uniform, and even originally smooth surfaces become rough with sputtering. Progressive development of roughness from an originally smooth surface is illustrated in Figure 3. Shortly after sputtering commences,

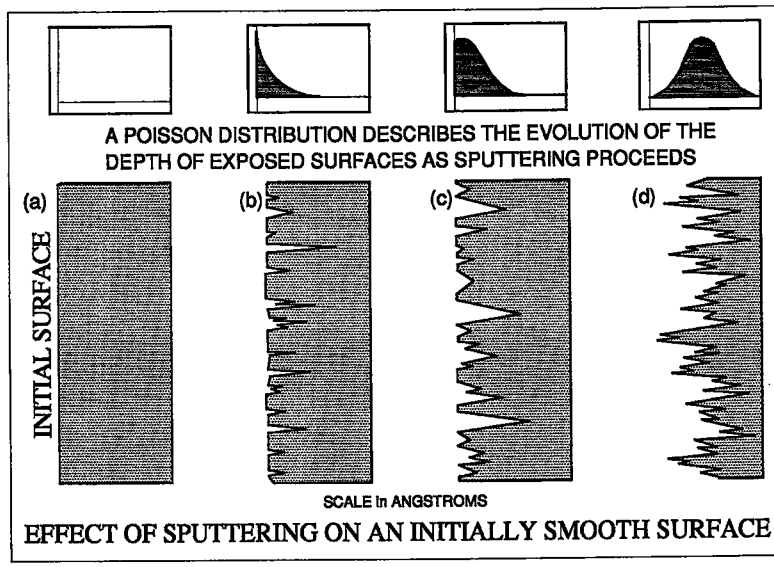

FIG. 3. Development, as a function of sputtering (and time), of a rough surface from an initially smooth surface. Depth of sputtering and surface roughness increase from left to right. The upper series of diagrams illustrates the distribution of surface exposed as a function of depth, at each stage of sputtering. The change in distribution of surface exposed, as a function of time, follows a Poisson distribution.

the initially flat surface still constitutes the majority of the exposed surface, but some of the interior of the sample also is exposed. With continued sputtering, progressively smaller amounts of the initial surface remain, and deeper portions of the solid constitute the greater proportion of the exposed surface. After sufficient sputtering, the initial surface is removed entirely, and the distribution of surfaces (with respect to depth) takes on a near-Gaussian distribution, which is retained for all subsequent sputtering. The change in the distribution of exposed surfaces as a function of depth is illustrated at the top of Figure 3. Development of rough surfaces produced by ion beams can be modeled statistically using the *Poisson distribution* (Fig. 3), and is the basis for interpreting compositional depth-profiles. The mean-free-path of an Auger electron dislodged from a specific element is effectively the escape-depth of the Auger electron for that element (Fig. 4). The escape-depth is dependent upon the nature of the matrix, energy of the emitted Auger electron, and the angle of emission of the Auger electron relative to the surface normal (Seah & Dench 1979). Escape-depths are different for each element and vary somewhat with the mineral (matrix) analyzed. The finite escape-depth of Auger electrons leads to attenuation of Auger depth-profiles, but the effects of attenuation can be calculated from a statistical model.

Bombardment of the surface by the ion beam causes atoms of the solid to be sputtered, and also causes *mixing* of atoms beneath the surface. Mixing includes implantation of atoms deeper into the solid (knock-on); atoms also may migrate closer to the surface, depending on the vagaries of the collisions. The effects on a contaminant layer in a solid are shown in Figure 5. The effect is to produce an Auger depth-profile that is representative of a dispersed layer of low concentration of contaminant, rather than a very thin layer of high concentration of contaminant.

Another effect that complicates the interpretation of Auger depth-profiles arises from the *preferential sputtering* of elements. Ion bombardment may cause the surface layers of some solids to decompose and may give rise to preferential sputtering of specific elements from the surface. The surface composition therefore is changed, and Auger analyses will not reflect the original composition of the surface. Steady-state conditions must be achieved (the residual layer must be built up to steady-state thickness) before reproducible results can be obtained, and before correction for preferential sputtering can be made. Electron or X-ray bombardment of the surface during analysis may change the oxidation state (reduction) of some elements, causing the solid to decompose or to be altered; consequently, bulk-composition data are more reliable than any data on chemical state obtained during depth profiling.

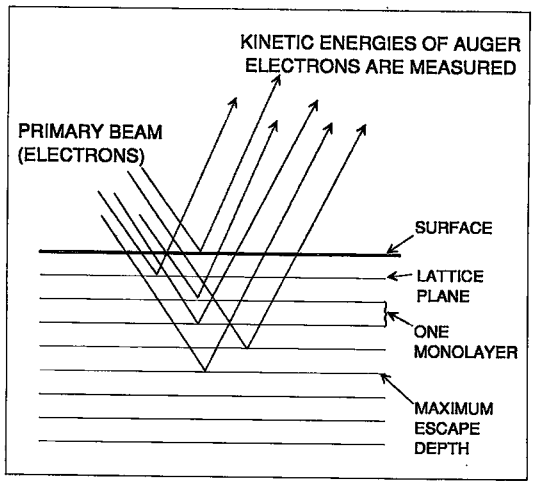

FIG. 4. Schematic illustration of incident electrons penetrating a solid surface and escape of the resulting Auger electrons from the uppermost few atomic layers of the solid. Only incident electrons giving rise to Auger electrons that escape the surface are illustrated here. Incident electrons, however, penetrate to a much greater depth than indicated in the diagram.

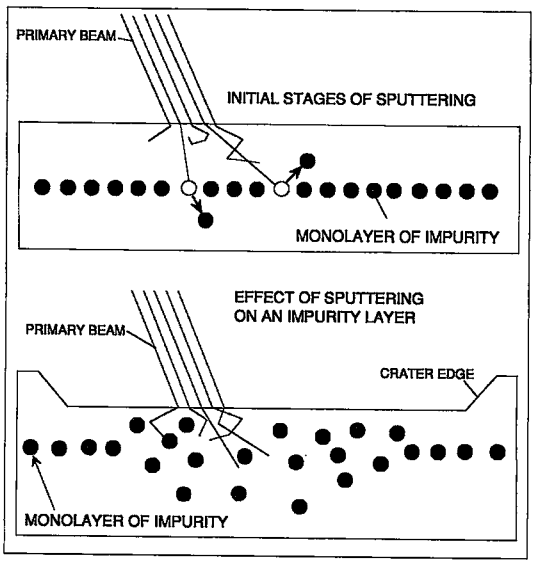

FIG. 5. The effects of incident-electron beam on a contaminant layer are shown. The path of incident electrons can be tortuous, resulting in dislodgment of contaminant atoms or ions from their original sites, and migration to both deeper and shallower depths. Note that the crater edge developed during sputtering is well removed from the region of the incident beam. This is assured by sputtering a much larger area than is analyzed.

Information on chemical states

Auger electrons released from a central ion are affected by surrounding atoms and ions, altering somewhat the kinetic energy of the Auger electrons. These shifts in kinetic energy can be used to obtain chemical information about elements in the near-surface of the solid. The information on chemical state includes oxidation state and, in some cases, the type of the nearest-neighbor species (to which the element is bonded). The difference in the kinetic energy of S^{6+} and S^{2-} is 4.7 eV (Fahlman *et al.* 1966), and should be detectable in most Auger spectra. Peak shapes also may provide information on chemical state (Quinto & Robertson 1971). Compared with XPS and X-ray emission spectroscopy, Auger data are more complex in that energies associated with three shells contribute to the Auger signal (hence, binding-energy calculations). Only one shell contributes to the XPS signal and two shells to the X-ray signal; thus these latter signals are easier to quantify and interpret. As a result, information on chemical state, although possible to obtain for some elements in solids, generally is not derived from Auger data. However, there are circumstances for which AES may be the only means to obtain information on chemical state. XPS uses a X-ray primary beam; the inability to focus the beam to a small size limits its application to natural systems. Where surfaces of individual grains are smaller than 1–2 mm, Auger may have to be used instead of XPS.

APPLICATIONS TO THE STUDY OF SOLID SURFACES

Introduction

Although there are few reported Auger spectroscopic studies of geological materials, there is now the opportunity and understanding to study these natural systems (Mogk & Locke 1988, Mogk 1990, Hochella *et al.* 1986, 1988, Hochella 1988). Semiconductors such as sulfides and some oxides do not charge appreciably, and can be analyzed accurately by Auger (Hochella *et al.* 1988, Pratt *et al.* 1994). Silicates, carbonates, sulfates and other salts are insulators and are subject to charging, but this has been overcome by judicious choice of the energy of the primary electron beam and the incident angle. Auger analyses of natural and experimentally leached silicates, including amphiboles and feldspars (Mogk & Locke 1988, Hochella *et al.* 1986, 1988) demonstrate the applicability of Auger analyses to nonconducting geological materials.

Bulk composition of goethite

Goethite is a Fe^{3+} oxyhydroxide of ideal composition FeO(OH). Electron-microprobe analyses of goethite from Tuscaloosa County, Alabama reveal

TABLE 1. CHEMICAL COMPOSITION OF GOETHITE

	1 Wt.%	2 Wt.%	3 Wt.%	4 Wt.%	5 Wt.%	6 Wt.%	Av. Wt.%	Diluted
Fe	59.15	59.64	61.18	60.95	61.84	61.10	60.64	
Mg	0.00	0.00	0.00	0.00	0.01	0.01	0.00	
Ca	0.00	0.00	0.01	0.00	0.00	0.00	0.01	
P	0.51	0.46	0.25	0.18	0.38	0.13	0.32	
Ba	0.00	0.00	0.01	0.04	0.00	0.03	0.01	
Al	0.15	0.17	0.07	0.22	0.18	0.20	0.17	
S	0.02	0.01	0.03	0.04	0.02	0.05	0.03	
Mn	0.07	0.03	0.07	0.02	0.01	0.07	0.05	
Na	0.00	0.06	0.01	0.03	0.00	0.03	0.02	
K	0.00	0.01	0.00	0.00	0.00	0.00	0.00	
F	0.63	0.71	0.75	0.69	0.70	0.65	0.69	
Cl	0.02	0.00	0.00	0.00	0.01	0.00	0.01	
TOTAL	60.55	61.09	62.38	62.18	63.15	62.27	61.94	
$FePO_4$	2.48	2.24	1.22	0.88	1.85	0.63	1.55	
AlO(OH)	0.33	0.38	0.16	0.49	0.40	0.44	0.37	
MnO_2	0.11	0.05	0.11	0.03	0.02	0.11	0.07	
FeOF	3.01	3.39	3.59	3.30	3.35	3.11	3.29	
FeO(OH)	89.69	90.24	93.11	93.22	94.02	93.79	92.34	
TOTAL	95.63	96.30	98.17	97.92	99.63	98.09	97.62	
H_2O (dif.)	4.37	3.70	1.83	2.08	0.37	1.91	2.38	
	At.%	At.%	At.%	At.%	At.%	At.%	At.%	At.%
Fe	30.25	30.66	31.95	31.81	32.52	31.95	32.06	27.56
P	0.47	0.43	0.24	0.17	0.36	0.12	0.22	0.19
Al	0.47	0.43	0.24	0.17	0.36	0.12	0.22	0.19
Mn	0.04	0.02	0.04	0.01	0.01	0.04	0.02	0.02
F	0.95	1.07	1.15	1.06	1.08	1.00	1.07	0.92
O	67.82	67.40	66.39	66.78	65.68	66.77	66.40	57.10

* Owing to the presence of appreciable concentrations of phosphorus and fluorine, the compositions are quoted in terms of elements rather than oxides to simplify presentation of subsequent calculations. The compositional data were obtained by electron-microprobe analysis.

appreciable Al, F and P (Table 1). Al may substitute for Fe, and F for OH. Phosphorus may be present as $FePO_4$, or the phosphate anion may substitute for OH. The former component is assumed here. The results of the analyses, recast into the components FeO(OH), AlO(OH), FeOF and $FePO_4$, give totals ranging from 94.43 to 99.63%. The shortfall probably is adsorbed or unbound H_2O. Evidence for this comes from the Auger studies where outgassing of goethite was so rapid that the sample had to be pumped for 24 hours before the vacuum was sufficient to transfer the sample to the analytical chamber. The atomic percentage of the elements are calculated assuming that unbound H_2O constitutes the difference between 100 weight % and sum of the percentages of the components FeO(OH), AlO(OH), FeOF and $FePO_4$ (Table 1).

Auger survey scans

The surface of goethite was gently sputtered for a short period (< 1 minute) to remove the bulk of the contaminants that had adhered to the surface. It is particularly important that adhered oxygen is removed, otherwise the Auger oxygen signal would include its contribution.

The integrated Auger survey scan of goethite (Fig. 2A) decreases between 30 and 100 eV, indicating slight charging of the sample. However, charging is insufficient to affect the Auger signal at kinetic energies greater than 150 eV. The survey scan records the presence of three major elements, oxygen, iron and carbon. The largest peak is oxygen at approximately 515 eV, with a smaller oxygen peak at 494 eV. There are three Auger peaks for Fe, at approximately 597, 652 and 705 eV, and a carbon peak at 271 eV. The integrated signal also indicates the presence of Al and Ni at 53 and 850 eV, respectively. These are more apparent in the differentiated signal (Fig. 2B). The Al peak is in the region affected by charging, and it is excluded from calculations of composition because it cannot be properly quantified.

Composition from survey scans

The composition of the near-surface region of goethite is calculated from the differentiated spectrum (Fig. 2B). Each Auger peak of the differentiated spectrum consists of an initial positive slope extending to a maximum, followed by a descending "middle arm" that terminates in a minimum, and a third arm with positive slope, rising to background values. The energies of the differentiated peaks are, by convention, taken at the peak minimum. Compositions are obtained by measuring the distance between the peak maximum and peak minimum (the length of the vertical component of the middle arm). The length of the middle arm of the oxygen peak at 511 eV is seven units (the peak scaled to maximum). The middle arm of the highest-energy Fe peak (705 eV) is used by convention to determine Fe content. Measurement of the length of the vertical component (amplitude) of the Fe, C and Ni peaks also is required to calculate the near-surface composition (Fig. 2B). The amplitude for each peak, modified only by the sensitivity factor for the element, is used to calculate relative atomic proportions. The equation generally used for this purpose is (Mogk 1990)

$$X_i = (I_i/S_i)/[\Sigma_j(I_j/S_j)] \quad (2)$$

where i is the element of interest, and j is the jth element (and includes i). X is the atomic fraction of the element, I is the peak-to-peak Auger amplitude of each element (*i.e.*, the length of the middle arm of the appropriate Auger peak of the element), and S is the sensitivity-factor for each element. The summation is carried out over all elements observed in the Auger spectrum (Fig. 2B). Numerous parameters contribute to sensitivity-factors (Palmberg 1976), and it is difficult to calculate accurate sensitivity-factors applicable to all solids. Fortunately, the problem is circumvented by use of mineral standards and prescribed instrumental conditions (Hochella *et al.* 1986).

Davis *et al.* (1976) quoted sensitivity-factors for Fe, O, C and Ni of 0.21, 0.50, 0.18 and 0.27, respectively (3 kV primary electron beam). These are obtained from Eq. (2) using native Fe metal, MgO, graphite and Ni metal as standards for the respective elements. Substitution of the Auger intensities and the respective

sensitivity-factors into Eq. (2) gives 31.7 atomic % Fe, 52.0% O, 13.0% C and 3.3% Ni. Electron-microprobe analyses No. 3 to No. 6 pertain to the least hydrated materials, and probably are most representative of the goethite sample analyzed by Auger (sample was degassed at 10^{-7} torr for 24 hours in the introduction chamber). The average atomic percentage of the four microprobe analyses are 32.06 Fe, 0.22 P, 0.22 Al, 0.02 Mn, 1.07 F and 66.40% O. Since the Auger analysis includes 13% C and 3.3% Ni, the *microprobe* result must be diluted by 16.3% to allow direct comparison with the AES result. After dilution, the average result of the microprobe analyses yields 27.6 and 57.1 atomic % Fe and O, respectively, compared with the Auger result of 31.7 and 52.0 atomic %. The difference is attributed to inaccurate sensitivity-factors for Fe and O. Sensitivity-factors calculated from Eq. (2) using the electron-microprobe analyses and Auger intensities are 0.227 and 0.428, respectively for Fe and O, whereas those of Davis *et al.* (1976) are 0.21 and 0.50.

Although the sensitivity-factors of Davis *et al.* (1976) give inaccurate compositions of goethite, Pratt *et al.* (1994) used these sensitivity-factors to obtain accurate proportions of Fe and S in pyrrhotite, demonstrating that sensitivity-factors are dependent upon the matrix (solid) being analyzed. The reviews of Hochella *et al.* (1988) and Mogk (1990) emphasize the need to use appropriate standards to obtain accurate data by Auger electron spectroscopy.

Auger and microprobe analyses indicate that Al is present in both the near-surface and in the bulk of the sample. The element may well substitute for Fe in the goethite structure as the solid formed. Auger spectroscopy indicates appreciable Ni in the near-surface of goethite, but electron-microprobe analyses reveal no detectable Ni. Nickel probably is adsorbed onto the surface but is absent from the interior (bulk phase).

Applications to Reacted Solid Surfaces

Introduction

Minerals reacted with air or natural solutions may undergo reaction and produce a leached or altered layer. The thickness of the altered layer, and its composition as a function of depth, can be obtained by Auger compositional depth-profiling. The information collected provides substantial insight into the rates of reaction and the mechanism by which reaction proceeds. Unfortunately, the Auger signal is attenuated by a number of processes, so that the collected profile may not mimic the true compositional changes within reacted layers. However, true compositions can be obtained through modeling of the depth profiles.

Proposed models from which depth-profiles are calculated must duplicate measured Auger depth-profiles to be feasible, but successful modeling of the profiles is not *sufficient* to prove a model correct. The sequential-layer sputtering model (SLS model) used here (Sanz & Hofmann 1986) is a statistical, trial-and-error model. It considers two important aspects: (1) development of surface roughness resulting from sputtering, and (2) escape-depths of individual elements. A quantitative treatment of each follows.

Depth profiles and surface roughness

Benninghoven (1973) and Hofmann (1976) considered the effects of surface roughness on attenuation of compositional depth-profiles and developed a model to account for attenuation by sputtering. In developing the model, they argued that sputtering occurs in the surface (exposed) layer only, and that sputtering yield is independent of local compositional variations within the material. Quantitative aspects now follow.

Consider a solid in which the atomic fraction of element i in the nth monolayer is denoted by $X_{i,n}$. After sputtering for some time, surface roughness has developed, exposing numerous monolayers, as in Figure 3. Each monolayer is exposed at a different depth and may be of different composition. The Auger signal of element i is determined by the atomic fraction of i in each monolayer ($X_{i,n}$), and by the percentage of the area that each monolayer n contributes to the total surface area. This percentage is given by a Poisson distribution (Gaussian distribution is achieved after some time; Fig. 3), and the total contribution to the Auger signal of i at time t [$X_i(t)$] is given by

$$X_i(t) = \Sigma_n X_{i,n} \cdot (1/n!) \cdot (n)^n \cdot e^{-n}. \quad (3)$$

Eq. (3) can be recast in terms of time rather than n (or depth) through the following relations. Let the thickness of a monolayer be a (Å), time be t (in seconds) and the sputter (or erosion) rate be z* (in monolayers/second). The depth, d (Å), to monolayer n is

$$d = n \cdot a \quad (4)$$

and the time taken to sputter to monolayer n is

$$t = d/z^* \quad (5)$$

Noting that $a/z^* = \tau$ and $n = t/\tau$, the integrated coverage of the total sample-surface, with respect to component i, after sputtering time t is

$$X_i(t) = \Sigma_n X_{i,n} \cdot (1/n!) \cdot (t/\tau)^n \cdot e^{(-t/\tau)} \quad (6)$$

Eq. (3) or (6) can be used to obtain atomic percentage of i as a function of either depth or time of sputtering.

The attenuation of a depth-profile due to surface roughness alone is shown in Figure 6. For this hypothetical example, element i is absent from the first 10 monolayers of the solid, but beyond 10 monolayers

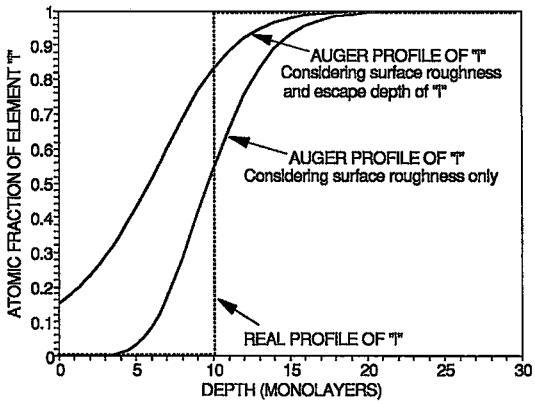

FIG. 6. The calculated attenuation effects, resulting from surface roughness and escape-depth, on the Auger depth-profile of element *i* in a solid. The curve showing the effects of surface roughness only is calculated from Eq. (6), and the curve showing the effects of both surface roughness and escape-depth is calculated from Eq. (7). Both curves are calculated assuming the elemental distribution of *i* indicated by the dashed line. Monolayer thickness is assumed to be 1 Å, and the escape-depth of *i* used in the calculation is 5.5 Å (the approximate value for Fe and O in pyrrhotite; Sanz & Hofmann 1986).

the solid is composed entirely of *i*. The dashed lines represent the real distribution of *i* in this solid. The solid curve is calculated from Eq. (3) and Eq. (6) assuming that surface roughness alone affects attenuation of the Auger profile. Surface roughness has a major effect on Auger profiles and must be considered when interpreting profiles.

Depth profiles and escape depths

The escape-depth (or attenuation length) of Auger electrons varies somewhat with individual elements and with matrix composition of the solid, but generally it is within the range of a few to a few tens of Ångströms (Seah & Dench 1979). As a result, the Auger signal for an element is derived not just from the surface layer but from subsurface layers as well. The effect is to attenuate Auger-depth profiles because the total Auger signal is integrated over a few monolayers. Equations (3) and (6) must be modified to accommodate the effect of escape-depth, and this is done by summing over all monolayers from which Auger electrons can be detected. The resulting equation (Sanz & Hofmann 1986) is

$$X_i(t) = \Sigma_m \Sigma_n X_{n+m} \cdot [n^{(n-1)}/(n-1)!] \cdot e^{-n} e^{(m/\lambda_i)}, \qquad (7)$$

where *m* represents the *m*th layer from which Auger electrons are generated, and λ_i is the escape-depth of element *i* in the solid being profiled. Σ_m represents the summation over 0 to *M* monolayers, where the practical limit to *M* is approximately 5 to 6 λ_i. Σ_n represents the summation over 1 to *N* monolayers, where *N* is sufficiently large that its truncation of the summation has no effect on X_i. Typically, *N* is double the total number of monolayers being modeled. The escape-depth (λ_i) used to calculate the profile of Figure 6 is 5.5 Å, which is the escape-depth of oxygen in an O- and S-bearing FeCrNi alloy (Sanz & Hofmann 1986, Fig. 9). The combined effects of surface roughness and escape-depth are shown in Figure 6; the calculation demonstrates that there will be a significant Auger signal for *i* (approximately 15 at.%) at the surface even though *i* is absent from the uppermost 10 Å. The signal will be observed in a survey scan of the surface before sputtering, and the signal increases rapidly as sputtering proceeds. Eq. (7) is used subsequently to interpret depth-profiles of air-oxidized pyrrhotite.

There is a third effect that may have to be considered when interpreting depth-profiles. Some elements may be sputtered in preference to others, but this can be compensated for by depth-profiling bulk standard samples of constant composition to determine the degree of preferential sputtering. Pyrrhotite was studied in this manner by Pratt *et al.* (1994), and they showed that sulfur is not sputtered in preference to iron.

AES DEPTH-PROFILES OF AIR-OXIDIZED PYRRHOTITE

Introduction

Pratt *et al.* (1994) studied the surface of air-oxidized pyrrhotite using XPS and AES; the AES results are shown in Figure 7. Pyrrhotite from Santa Eulalia, Chihuahua, Mexico was selected for study. Pratt *et al.* (1994) collected 34 analyses of the pyrrhotite, the average composition of which is 46.44 at.% Fe and 53.6% S, respectively, *i.e.*, very close to Fe_7S_8. An X-ray-diffraction study indicated a mixture of monoclinic and hexagonal structures. A sample was fractured along the (001) parting plane. The surface was irregular on a large scale (25× magnification), but individual surfaces many tens of μm on a side were observed to be smooth at 1000× magnification by SEM, and remained smooth after 50 hours of air oxidation. Survey scans were taken of 1 μm^2 surfaces before sputtering, and after sputtering was complete.

The survey scan of the air-oxidized pyrrhotite prior to sputtering shows C, O, S and Fe. A test profile was collected, and carbon disappeared after the first sputtering interval. As a result, subsequent depth-profile analysis was restricted to Fe, S and O. Sputter intervals between analyses were 10 seconds, and sputter rate was 40 Å per minute (measured with a Sloan Dectak II™

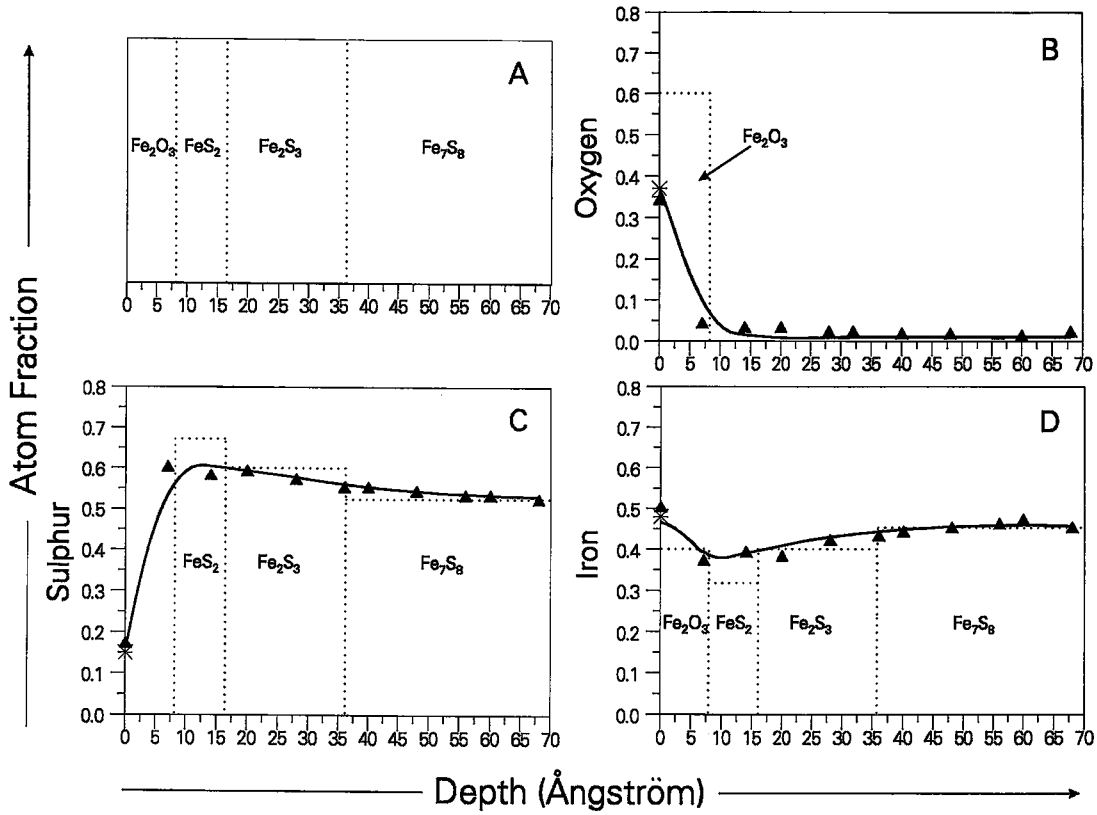

FIG. 7. Modeled and analyzed depth-profiles of 50-hour air-oxidized pyrrhotite (Pratt *et al.* 1994) where each compositional zone is of fixed composition. (A) The results of the sequential-layer sputtering model (SLS) calculations of 50-hour air-oxidized pyrrhotite. (B) The analytical data and results of modeling for oxygen. (C) The analytical data and results of modeling for sulfur. (D) The analytical data and results of modeling for iron. The triangles of Figures 7B, C and D are the analytical Auger data. The dashed lines of Figures 7B, C and D delineate the composition and thickness of the respective element in the proposed layer. The solid curve in each diagram is the depth-profile calculated from Eq. 7 using the proposed model of Fig. 7A. The escape-depths used for O, S and Fe are 5.5, 2.6 and 5.4 Å, respectively (Sanz & Hofmann 1986), and a monolayer is 2 Å thick (calculated from the unit-cell parameters).

stylus-type profilometer. All profiles are plotted as a function of depth.)

Depth profiles

Compositional depth-profiles for O, S and Fe of pyrrhotite exposed to the atmosphere for 50 hours (Figs. 7B, C and D; triangles represent results of individual Auger analyses) show that oxygen is high in the near-surface (36 at. %) but decreases rapidly to very low values within 10 Å of the surface (Fig. 7B). The sulfur profile (Fig. 7C) shows low S in the near-surface region (17 at.%), and a rapid increase with depth to a maximum value (near 60 at.%) at intermediate depths, followed by a slow decline to values representative of bulk pyrrhotite (54 at.%) at depth. Iron (Fig. 7D) gives a high signal at the surface (49 at.%), decreases to a minimum (37 at.%) near 5 to 20 Å, and rises slowly to the value for bulk pyrrhotite (46 at.% Fe).

These data show that there is an Fe-oxide-enriched layer at the surface, probably 5 to 10 Å thick. X-ray photoelectron spectra show that Fe^{3+}–O species predominate at the surface, with electron binding energies similar to those of hematite (Pratt *et al.* 1994, McIntyre & Zetaruk 1977). Beneath the oxide layer is a layer enriched in S and depleted of Fe relative to bulk pyrrhotite (Fe_7S_8). Jones *et al.* (1992) also detected a sulfur-rich layer in the near-surface region of oxidized pyrrhotite, corroborating the Auger depth-profile results (Fig. 7). Although the conclusion that there are

three layers present is not in doubt, little quantitative can be said about the thicknesses or compositions of the layers without accounting for attenuation of the Auger depth-profile.

Modeled profiles in pyrrhotite

The sequential-layer sputtering (SLS) equations (Sanz & Hofmann 1986, and Eq. 7) are used here to extract additional quantitative data. Use of the SLS calculation first requires construction of a model of the near-surface, with composition and thickness of each zone specified. The depth-profiles for Fe, S and O then are calculated from the model, taking into account the effective roughness of the surface and escape-depth (Eq. 7). Comparison of the calculated profiles with the Auger data provides the test of the feasibility of proposed model.

XPS shows a Fe^{3+}–oxide layer at the surface, the composition of which is taken as Fe_2O_3. The layer is thin, as indicated by the oxygen Auger depth-profile (Fig. 7B); consequently, a Fe_2O_3 layer 8 Å thick is proposed for the model. The Auger profile for sulfur (Fig. 7C) shows a maximum S content between 5 and 20 Å, and suggests the presence of a S-rich zone beneath the oxide layer. Jones *et al.* (1992) noted a sulfur-rich layer in the near-surface of pyrrhotite, and argued that its composition may approach FeS_2. This model considers the sulfur-rich zone to have a composition of FeS_2 and to extend from 8 to 16 Å in depth. Another zone, more sulfur-rich than bulk pyrrhotite, but of lower sulfur content than FeS_2, and extending to a depth of approximately 40 Å, is required to model successfully the Auger results (Fig. 7A). Jones *et al.* (1992) suggested that Fe_2S_3 occurs in the near-surface of oxidized pyrrhotite, and this composition, extending from 16 to 36 Å in depth, is adopted for the SLS model. Bulk pyrrhotite occurs at depth greater than 36 Å. The compositional zones used for the SLS model are summarized in Figure 7A. The compositional depth-profiles for Fe, S and O (Fig. 7, solid curves) calculated using the proposed model agree reasonably well with the Auger analytical data (Fig. 7, triangles), and the proposed model is considered feasible. We note, however, that other models also yield agreement with the analytical data, as now emphasized.

The previous SLS model was constructed assuming that each zone is of unique and constant composition. This represents the traditional approach to SLS modeling (Sanz & Hofmann 1986). However, if it is assumed that zones are of variable composition, another SLS model can be constructed. An outermost 8 Å layer of Fe_2O_3 (Fig. 8A) overlies a sulfur-rich layer, the sulfur content of which decreases continually from the contact with the oxide layer to bulk composition of the pyrrhotite at a depth of 40 Å. The calculated SLS profile (Figs. 8B, C and D, solid curves) shows as good agreement with the analytical data as the first model, and there are no grounds to choose one model over the other.

Important information is obtained from the exercise regardless of the model adopted. There is a Fe^{3+}-oxide layer, approximately 8 Å thick, on the surface of pyrrhotite. A sulfur-rich layer extending from 8 to 35–40 Å separates the oxide layer and bulk pyrrhotite. The portion of the sulfur-rich zone closest to the oxide layer is richest in S, and approaches the composition FeS_2, with sulfur and iron contents of 65 to 70 at. %, and 30 to 35%, respectively, observed at the contact with the oxide layer. At a depth of 20 Å, the S has decreased to approximately 60%, and Fe has increased to 40%. Finally, oxygen is absent at depths greater than 8 Å. These are important quantitative data which, combined with results of others, provide insight into the mechanism of oxidation of pyrrhotite (Pratt *et al.* 1994). Aspects related to mechanism now are summarized.

The Auger depth-profiles show that a few monolayers of oxygen have accumulated at the pyrrhotite surface during the 50-hour exposure to the atmosphere (Pratt *et al.* 1994). Molecular oxygen of the atmosphere is adsorbed rapidly onto the surface, where it is reduced to O^{2-} (Roberts 1991, Buckley & Woods 1985, Jones *et al.* 1992, Pratt *et al.* 1994). Electrons involved in reduction are derived from the underlying pyrrhotite by oxidation of S^{2-} to di- and polysulfides (Pratt *et al.* 1994, Mycroft *et al.* 1995) or by oxidation of Fe^{2+} to Fe^{3+}. The Auger results and other evidence (Pratt *et al.* 1994) suggest that once a monolayer of Fe^{3+}-oxide is produced, electrons diffuse from the underlying pyrrhotite, through the oxide layer, to reduce O_2 adsorbed onto the recently formed oxide layer; Fe diffuses through the oxide layer to form a new monolayer of Fe^{3+}-oxide at the surface (on the previously formed oxide layer). Progressive thickening of the oxide layer should slow its rate of formation as electrons and Fe must diffuse through an ever-thickening oxide layer (provided diffusion is the rate-limiting process). Auger and other data indicate that the rate of formation of the Fe^{3+}-oxide layer is very rapid initially and decreases with time (Pratt *et al.* 1994). After some time, pyrrhotite oxidation may occur *via* mechanisms other than the one proposed here, and long-term leaching studies are required to investigate this possibility.

In summary, Auger depth-profiling has an obvious advantage over many other depth-profiling techniques; quantitative analysis of samples for both major and minor elements can be obtained at the Ångström scale. Although other techniques, such as secondary ion mass spectrometry (SIMS), give compositional depth-profiles, they require greater preparation (*e.g.*, ion implantation of each element to be quantified) to obtain quantitative results. Auger spectroscopy is perhaps the most useful technique for quantitative study of altered surfaces of minerals.

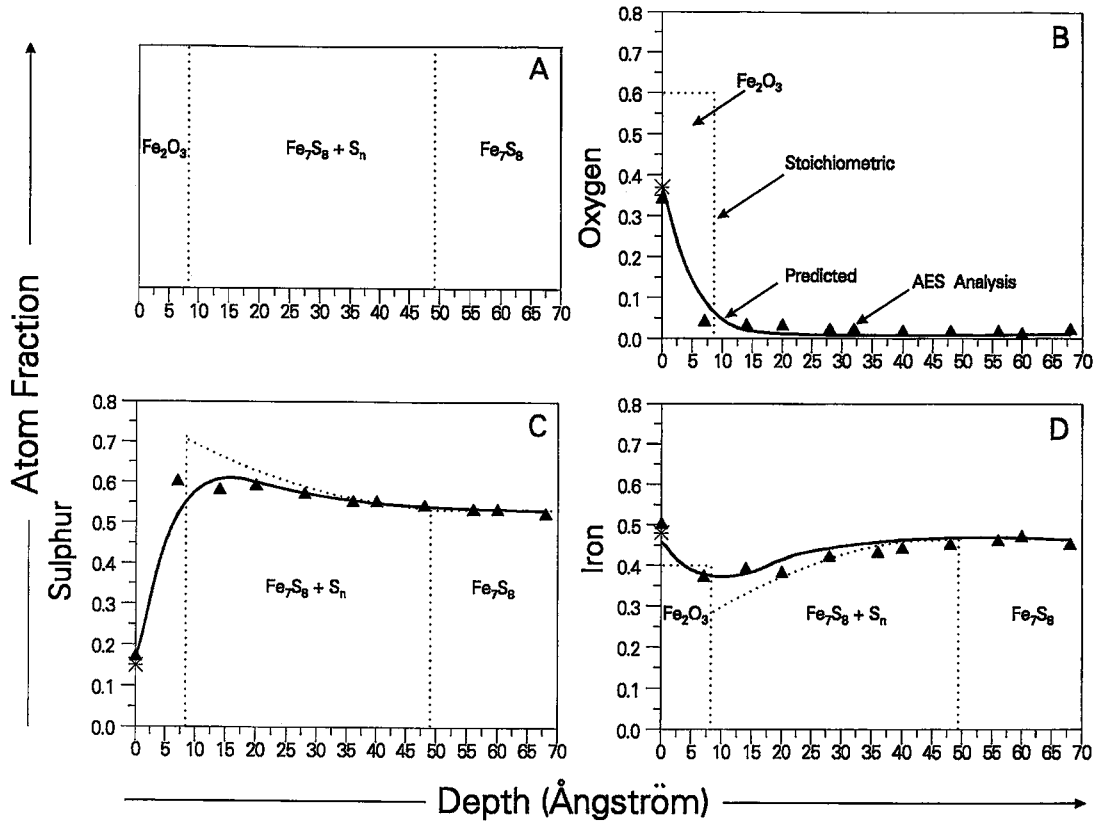

FIG. 8. Modeled and analyzed depth-profiles of 50-hour air-oxidized pyrrhotite (Pratt *et al.* 1993) where each compositional zone is of fixed composition. (A) The results of the sequential-layer sputtering model (SLS) calculations of 50-hour air-oxidized pyrrhotite. (B) The analytical data and results of modeling for oxygen. (C) The analytical data and results of modeling for sulfur. (D) The analytical data and results of modeling for iron. The triangles of Figures 8B, C and D are the analytical Auger data. The dashed lines of Figures 8B, C and D delineate the composition and thickness of the respective element in the proposed layer. The solid curve in each diagram is the depth-profile calculated from Eq. 7 using the proposed model of Fig. 8A. The escape-depths used for O, S and Fe are 5.5, 2.6 and 5.4 Å, respectively (Sanz & Hofmann 1986), and a monolayer is 2 Å thick (calculated from unit-cell parameters).

Constraints on modeling

Accurate elemental analysis of solids is dependent upon bulk composition of the solid analyzed (the matrix), primarily because Auger sensitivity-factors vary according to matrix composition. If the Fe^{3+}-oxide developed on the surface of pyrrhotite (Fig. 7) were much thicker, for example, different sensitivity-factors would have to be applied to the FeS-rich and the Fe–O-rich parts of the profile (see discussion of Fe and O sensitivity-factors for pyrrhotite and goethite in a previous section). Although crucial to quantification of profiles, this aspect has received little attention (Lorang *et al.* 1992), and procedures for derivation of appropriate sensitivity-factors generally have not been adequately described. A simple procedure is proposed here, and the air-oxidized pyrrhotite results (Fig. 7) are used as an example.

The sensitivity-factors for Fe and O in goethite are 0.227 and 0.428 (see section on goethite), whereas those for pyrrhotite are 0.21 and 0.50 (Davis *et al.* 1976); these values should be used where the minerals goethite and pyrrhotite are analyzed or where thick compositional zones of these species are present. In regions of depth-profiles where there are contributions from both species [FeO(OH) and FeS], the sensitivity-factor is calculated on the basis of proportion of each species contributing to the Auger signal of each element; consequently, the sensitivity-factor for oxygen is:

$$SF_O = 0.428X_{Gt} + 0.50X_{Po} \quad (8a)$$

and that for Fe is

$$SF_{Fe} = 0.227X_{Gt} + 0.21X_{Po} \quad (8b)$$

where SF_O and SF_{Fe} are the sensitivity-factors for oxygen and iron, and X_{Gt} and X_{Po} are the fractional molar contributions of goethite and pyrrhotite species to each element. SF_O and SF_{Fe} are referred to subsequently as *dynamic sensitivity-factors* to distinguish them from sensitivity-factors derived from pure phases (*i.e.*, standards). Once obtained, these dynamic sensitivity-factors (SF) are substituted for S in Eq. (2). The fractional contribution of each composition [FeO(OH) and Fe_7S_8] can be determined by comparing the intensity (counts) of the Auger signal for oxygen in the zoned sample with the Auger signal for oxygen in pure goethite, and similarly for S by comparing the signal in the zoned sample with the S signal of pure pyrrhotite. The approach has been proposed by Lorang *et al.* (1992), but it is difficult and tedious to use in that precisely the same operating conditions *and* the same surface properties must exist for the compositionally zoned and standard samples. It is not suited to the study of natural samples because the surface properties of naturally weathered or experimentally leached samples are unlikely to be the same as surfaces of the standards. Another, more practical, approach is described here.

Atomic percentages of sulfur and oxygen can be used to determine the fractional contribution of each species [FeO(OH) and Fe_7S_8] to the Auger signal. The fractional contribution of Fe_7S_8 (X_{Po}) is given by S/(S + O/2) and X_{Gt} by (O/2)/(S + O/2), where S and O are the atomic fractions of S and O from the Auger analysis. Division by 2 arises because two atoms of oxygen are present per formula unit of FeO(OH). Once S and O have been obtained, X_{Po} and X_{Gt} can be calculated, and the dynamic sensitivity-factors can be determined from Eq. (8). The factors then are substituted into Eq. (2) to obtain better estimates of the atomic fractions of S and O. The calculations are started by substituting sensitivity-factors for either standard (goethite or pyrrhotite) into Eq. (2) to obtain first estimates of the mol fraction of each species. The entire calculation is repeated (iterative calculation) using the updated estimates of mol fractions and dynamic sensitivity-factors until convergence of composition is achieved.

Summary

Auger analysis is most useful for study of major- and minor-element compositions of Ångström-thick surface layers, where μm-scale lateral resolution is required. The ability to observe surface textures and morphology at high magnification, coupled with the extreme surface-sensitivity and excellent lateral resolution, make Auger spectrometry one of the most useful analytical tools with which to study mineral surfaces. It is particularly valuable to study mineral–solution interactions at low temperatures, where reaction rates commonly are slow, as Auger spectrometry can detect reactions that have affected only a few atomic layers near the surface of solids.

A continual problem with hydrothermal experimental studies is detection of product phases. Traditional methods (optical microscopy coupled with X-ray diffraction or electron-microprobe analysis) require appreciable extents of conversion to be certain that one assemblage has formed at the expense of the other. Auger instruments can be used to both detect small amounts of secondary products in scanning mode (Scanning Auger Microscopy) and to analyze Ångström-thick products less than a μm in diameter.

Perhaps the greatest potential for geological studies arises with the ability to obtain Ångström-scale compositional depth-profiles with lateral resolution of a μm. The study of oxidized pyrrhotite described here is an example where Auger provides analytical results that cannot be easily collected by any other technique. The Auger results, coupled with XPS, provide insight into transport processes at mineral–solution interfaces and insight into reaction mechanisms of minerals in solution.

Auger spectrometry has many applications in the Earth Sciences, and in the future, it will be a standard geochemical tool. For the moment, its application is limited primarily by a general lack of knowledge of its usefulness, and by accessibility. This will change as more Earth scientists use the technique, and demand to have Auger instruments available in Earth Science departments.

Acknowledgements

We thank M.F. Hochella, D.W. Mogk, R.F. Martin and F.C. Hawthorne for editing the manuscript. Special thanks are extended to F.C. Hawthorne for his detailed editorial comments and suggestions for improvements to the manuscript. These reviewers have added substantially to the organization, content and presentation of the paper. Grants from the Natural Sciences and Engineering Research Council of Canada (NSERC) and from the Prediction Committee of MEND (Mining Environment and Neutral Drainage, CANMET) funded the research reported here.

References

Auger, P. (1925): Sur les rayons β secondaires produits dans un gaz par des rayons X. *C.R. Acad. Sci.* **180**, 65-68.

Benninghoven, A. (1973): New developments in the surface analysis of solids. *Appl. Phys.* **1**, 3-8.

BRIGGS, D. & SEAH, M.P. (1990): Spectral interpretation. *In* Practical Surface Analyses (2nd ed.). **1**. Auger and X-ray Photoelectron Spectroscopy (D. Briggs & M.P. Seah, eds.). J. Wiley and Sons, New York, N.Y. (85-142).

BUCKLEY, A.N. & WOODS, R. (1985): X-ray photoelectron spectroscopy of oxidized pyrrhotite surfaces. I. Exposure to air. *Appl. Surf. Sci.* **22/23**, 280-287.

BURHOP, E.H.S. (1952): *The Auger Effect and Other Radiationless Transitions.* Cambridge Univ. Press, Cambridge, U.K.

_____ & ASSAD, W.M. (1972): Auger effect. *Adv. Atom. Mol. Phys.* **8**, 163-284.

CARLSON, T.A. (1975): *Photoelectron and Auger Spectroscopy.* Plenum Press, New York, N.Y.

DAVIS, L.E., MACDONALD, N.C., PALMBERG, P.W., RIACH, G.E. & WEBER, R.E. (1976): *Handbook of Auger Electron Spectroscopy* (2nd ed.). Physical Electronics Industries, Eden Prairie, Minnesota.

FAHLMAN, A., HAMRIN, K., HEDMAN, R., NORDBERG, R., NORDLING, C. & SEIGBAHN, K. (1966): Electron spectroscopy and chemical bonding. *Nature* **210**, 4-8.

HOCHELLA, M.F., Jr. (1988): Auger electron and X-ray photoelectron spectroscopies. *In* Spectroscopic Methods in Mineralogy and Geology (F.C. Hawthorne, ed.). *Rev. Mineral.* **18**, 573-638.

_____, HARRIS, D.W. & TURNER, A.M. (1986): Scanning Auger microscopy as a high-resolution microprobe for geologic materials. *Am. Mineral.* **71**, 1247-1257.

_____, PONADER, H.B., TURNER, A.M. & HARRUS, D.W. (1988): The complexity of mineral dissolution as viewed by high resolution scanning Auger microscopy: labradorite under hydrothermal conditions. *Geochim. Cosmochim. Acta* **52**, 385-394.

HOFMANN, S. (1976): Evaluation of concentration-depth-profiles by sputtering in SIMS and AES. *Appl. Phys.* **9**, 59-66.

_____ (1990): Depth profiling in AES and XPS. *In* Practical Surface Analyses (2nd ed.). **1**. Auger and X-ray Photoelectron Spectroscopy (D. Briggs & M.P. Seah, eds.). J. Wiley and Sons, New York, N.Y. (143-200).

JONES, C.F., LECOUNT, S., SMART, R.St.C. & WHITE, T. (1992): Compositional and structural alteration of pyrrhotite surfaces in solution: XPS and XRD studies. *Appl. Surf. Sci.* **55**, 65-85.

KIM, K.S., GAARENSTROOM, S.W. & WINOGRAD, N. (1976): Calculation of $L_{2,3}M_{45}M_{45}$ Auger energies of metallic Ni, Cu and Zn. *Chem. Phys. Lett.* **41**, 503-506.

LANDER, J.J. (1953): Auger peaks in the energy spectra of secondary electrons from various materials. *Phys. Rev.* **91**, 1382-1387.

LORANG, G., XU, J.L. & LANGERON, J.-P. (1992): Quantitative AES depth profiling of thin oxide films grown on stainless steels and aluminium. *Surface and Interface Anal.* **19**, 60-64.

MACDONALD, N.C. (1970): Auger electron spectroscopy in scanning electron microscopy: potential measurements. *Appl. Phys. Lett.* **16**, 76-80.

MCINTYRE, N.S. & ZETARUK, D.G. (1977): X-ray photoelectron spectroscopic studies of iron oxides. *Anal. Chem.* **49**, 1521-1529.

MEHLHORN, W. (1970): *The Auger Effect.* Report from the Behlen Lab. of Physics, Univ. of Nebraska, Lincoln, Nebraska.

MOGK, D.W. (1990): Application of Auger electron spectroscopy to studies of chemical weathering. *Rev. Geophys.* **28**, 337-356.

_____ & LOCKE, W.W. (1988): Application of Auger electron spectroscopy (AES) to naturally weathered hornblende. *Geochim. Cosmochim. Acta* **52**, 2537-2542.

MYCROFT, J.R., NESBITT, H.W. & PRATT, A.R. (1995): X-ray photoelectron and Auger electron spectroscopy of air-oxidized pyrrhotite: distribution of oxidized species with depth. *Geochim. Cosmochim. Acta* **59**, (in press).

PALMBERG, P.W. (1976): Quantitative Auger electron spectroscopy using elemental sensitivity factors. *J. Vac. Sci. Technol.* **13**, 214-218.

_____, BOHN, G.K. & TRACY, J.C. (1969): High sensitivity Auger electron spectrometer. *Appl. Phys. Lett.* **15**, 254-255.

PLEASONTON, F. & SNELL, A.H. (1957): Ionization following internal conversion in xenon. *Proc. R. Soc. London* **241A**, 141-152.

PRATT, A.R., MUIR, I.J. & NESBITT, H.W. (1994): X-ray photoelectron and Auger electron spectroscopic studies of pyrrhotite and mechanism of air oxidation. *Geochim. Cosmochim. Acta* **58**, 827-841.

QUINTO, D.T. & ROBERTSON, W.D. (1971): Identification of Auger spectra from aluminum. *Surf. Sci.* **27**, 645-648.

RIVIÈRE, J.C. (1990): Instrumentation. *In* Practical Surface Analyses (2nd ed.). **1**. Auger and X-ray Photoelectron Spectroscopy (D. Briggs & M.P. Seah, eds.). J. Wiley and Sons, New York, N.Y. (19-84).

ROBERTS, M.W. (1991): Evidence for the role of surface transients and precursor states in determining molecular pathways in surface reactions. *Appl. Surf. Sci.* **52**, 133-140.

SANZ, J.M. & HOFMANN, S. (1986): Quantitative AES depth profiling of very thin overlayers. *Surf. Interface Anal.* **8**, 147-157.

SCHEIBNER, E.J. & THARP, L.N. (1967): Inelastic scattering of low energy electrons from surfaces. *Surf. Sci.* **8**, 247-265.

SEAH, M.P. & DENCH, W.A. (1979): Quantitative electron spectroscopy of surfaces: a standard data base for electron inelastic mean free paths in solids. *Surf. Interface Anal.* **1**, 2-11.

SEVIER, K.D. (1972): *Low Energy Electron Spectrometry.* Wiley-Interscience, New York, N.Y.

WEBER, R.E. & PERIA, W.T. (1967): Use of LEED apparatus for the detection and identification of surface contaminants. *J. Appl. Phys.* **38**, 4355-4358.

WELLS, O.C. & BREMER, C.G. (1969): Improved energy analyzer for the scanning electron micropscope. *J. Sci. Instrum.* **2**, 1120-1121.

Received June 10, 1993, revised manuscript accepted April 14, 1994